Adsorption of CO_2 on Model Surfaces of Cesium Oxides Determined from First Principles

Jianren Tai, Qingfeng Ge,† Robert J. Davis,* and Matthew Neurock*

Department of Chemical Engineering, University of Virginia, Charlottesville, Virginia 22904

Received: March 10, 2004; In Final Form: August 19, 2004

Gradient-corrected periodic density functional theory was used to examine the bulk and low index surfaces of several cesium oxides (Cs_2O, Cs_2O_2, and CsO_2). The adsorption of CO_2 on those surfaces was explored. The cesium-terminated {001} surface of Cs_2O had a weak affinity for CO_2 with an adsorption strength of only -4.1 kJ mol^{-1}. In contrast, the Cs_2O {010} surface exposing both Cs and O atoms adsorbed CO_2 with a strength of -284 kJ mol^{-1}. The adsorption of CO_2 in the bridged configuration on the {001} and the {100} surfaces of Cs_2O_2 exhibited adsorption strengths of -101 and -186 kJ mol^{-1}, respectively. The oxygen-rich CsO_2 surface failed to adsorb CO_2. Results from a Mulliken charge analysis are consistent with the traditional ranking of basicity: $Cs_2O > Cs_2O_2 > CsO_2$.

1. Introduction

Oxides of cesium are used as photocathodes[1−6] and solid base catalysts for chemical reactions.[7,8] Solid bases also adsorb CO_2 and may eventually serve as CO_2 sequestration agents for emission gas control.[9−11] Incorporation of basic compounds on a support increases the surface area available for adsorption and chemical reactions. Zeolites containing occluded basic oxides are particularly interesting because of the unique microporous structures of zeolites with very high internal surface areas. When cesium acetate is impregnated into zeolites and decomposed to form an occluded oxide, the resulting solid exhibits catalytic activity in reactions such as double bond isomerization, toluene alkylation with methanol, and aldol condensation.[12−15] Studies have shown that the active sites are located inside the zeolite micropores.[16−19] However, the form of the occluded cesium oxide remains elusive. Hathaway and Davis suggested the presence of cesium oxide inside the zeolite supercages during their study of the 2-propanol dehydrogenation reaction over cesium-modified materials.[19] In their studies, no evidence of cesium metal, cesium carbonate, or cesium hydroxide was found after the calcination of the cesium acetate impregnated into zeolites X and Y. However, cesium oxide may be present in many forms inside the zeolite micropore, with possible compositions being stoichiometric cesium oxide (Cs_2O), cesium peroxide (Cs_2O_2), or cesium superoxide (CsO_2). Hathaway and Davis did not determine the form of the cesium oxide, but instead denoted the active site as Cs_xO_y.

Experimental attempts to elucidate the nature of these occluded species (hereby denoted as CsO_x) have been inconclusive. Because of the basic nature of CsO_x, CO_2 adsorption was used to characterize the strength of the basic adsorption sites. Lasperas et al. conducted a series of CO_2 temperature programmed desorption (TPD) experiments on X and Y zeolites containing occluded cesium.[18] On the basis of their measured 1:2 ratio of CO_2:Cs and assuming that adsorption proceeds through the reaction $Cs_2O + CO_2 \rightarrow Cs_2CO_3$, they concluded that the species inside the zeolite supercages was Cs_2O. Yagi and Hattori reached a similar conclusion on the basis of their results from TPD of CO_2 combined with isotopic oxygen exchange.[17] In a more recent study, Bordawekar and Davis found that only one CO_2 molecule adsorbed per four occluded cesium atoms in cesium ion modified zeolites CsX and CsY.[20] In addition, the adsorption enthalpy of CO_2 on CsO_x loaded into zeolites X and Y was about -85 kJ mol^{-1}. Interestingly, a bulk "Cs_2O" commercial sample was found to have a much higher CO_2 adsorption enthalpy of -270 kJ mol^{-1} after thermal treatment.[20] Since Krawietz et al. showed that commercially available "Cs_2O" is actually a mixture of Cs_2O_2 and CsO_2,[21] there is no reliable value of the CO_2 adsorption enthalpy on the stoichiometric oxide in the literature. Clearly, the form of CsO_x affects the adsorption energy of CO_2 on the different cesium oxide surfaces, and there is little experimental evidence to explain such an effect.

To help resolve some of these issues, we have used first-principles quantum chemical calculations to investigate the stability of various cesium oxide surfaces as well as the adsorption of CO_2 on these surfaces. Periodic density functional theory has been successfully applied to a wide range of studies for the adsorption and reaction of probe molecules over both pure metal and metal oxide surface.[22−29] The experimentally observed adsorption strength of CO_2 on different oxide surfaces is compared to the computational results for CO_2 on model cesium oxide surfaces to provide insights about the nature of supported CsO_x species. To the best of our knowledge, these results represent the first systematic exploration of the energetics of cesium oxide surfaces with and without adsorbed CO_2.

2. Computational Methods

Gradient-corrected density functional theory calculations were performed using the CASTEP code.[30−32] The electron−ion interactions were described by ultrasoft pseudopotentials.[33] The exchange/correlation energies were calculated using the Perdew−Wang form of the generalized gradient approximation (PW-GGA).[34] Using a 300 eV plane wave basis set cutoff, the calculated CO_2 bond length was 1.169 Å, in agreement with the experimental value of 1.160 Å.[35] This cutoff energy was used throughout our calculations.

* Corresponding authors. E-mail: R.J.D., rjd4f@virginia.edu; M.N. mn4n@virginia.edu.

† Current address: Department of Chemistry and Biochemistry, Southern Illinois University, Carbondale, IL 62901.

10.1021/jp048933v CCC: $27.50
Published on Web 10/02/2004

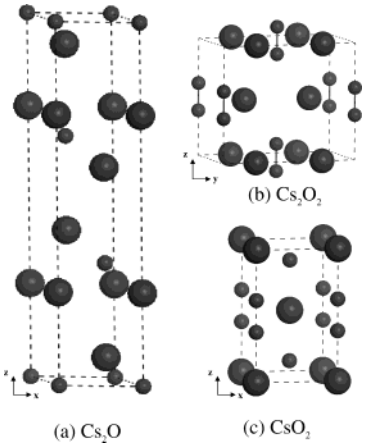

Figure 1. Bulk unit cell of CsO_x crystals. The large spheres represent cesium atoms and the smaller ones represent oxygen atoms.

Various structures of the bulk cesium oxides were examined. The unit cell of each oxide was initially constructed from known X-ray crystallographic data. The unit cell dimension and the position of Cs and O ions were then geometrically optimized. Slabs were constructed on the basis of the optimized unit cell of different cesium oxides. Several low index surfaces were subsequently exposed by making appropriate cuts through the slab. A vacuum space of 12 Å was created above each exposed surface. Carbon dioxide molecules were then placed at various adsorption sites on one side of the slab to calculate the adsorption structure and binding energy.

The Brillouin zone of the surface unit cell was sampled with a 3 × 3 Monkhorst−Pack mesh[36] for Cs_2O_2 and Cs_2O and a 3 × 5 Monkhorst−Pack mesh for CsO_2. The calculations for the CsO_2 surfaces were carried out using spin polarization to appropriately treat unpaired electrons that might result from the O_2^- surface states. In addition spin polarization calculations were carried out to test whether spin was important for modeling the systems where atomic oxygen is adsorbed to the Cs_2O surface. The results indicate that influence of spin was negligible. We expect these results to carry over to all of the systems examined herein. The calculations for all other surfaces and adsorption systems were therefore performed without spin polarization. Except for time-reversal symmetry, no further symmetry was imposed. The atoms in the bottom layer were fixed but all of the other atoms in the slab, as well as C and O atoms in CO_2 were allowed to relax according to the calculated Hellmann−Feynmann forces. After optimization, a Mulliken charge analysis was performed.[37]

The surface energy was calculated for stoichiometric slabs by the following equation:

$$E_{\text{surface}} = \frac{\left| \frac{E_{\text{optimized bulk unit cell}}}{\text{no. of stoichiometric units}} \times \text{no. of units in slab} - E_{\text{optimized slab}} \right|}{A_{\text{exposed surface}}}$$

E_{surface} represents the absolute value of the difference between the total energy of the optimized bulk unit cell and the optimized slab for a particular surface.

3. Results and Discussion

3.1. Crystal Structures of CsO_x. The crystal structures for three different cesium oxides, namely, Cs_2O, Cs_2O_2, and CsO_2, were optimized and subsequently compared to the structures established by XRD.[38] Figure 1 illustrates the bulk crystal unit cell of each compound. The Cs_2O crystal unit cell is a hexagonal *anti*-$CdCl_2$ type layer structure, which consists of three Cs−O−Cs triple layers.[39] The layers are weakly bound through van der Waals interactions. In each triple layer structure, an O atom is coordinated to five Cs atoms. Among the five Cs atoms, one is completely inside the unit cell and the other four occupy positions at the edge of the unit cell, shared with adjoining cells. The geometry provides a stoichiometry of two Cs atoms per O atom, as illustrated in Figure 1a. The Cs_2O_2 unit cell is orthorhombic and consists of two O−Cs−O triple layers.[40] There are two O atoms coordinated to two Cs atoms in each triple layer, as illustrated in Figure 1b. It has been shown that the crystallographic phase of α-CsO_2 is tetragonal, *I*4/*mmm*, at temperatures below ca. 368 K.[21] Above 368 K, α-CsO_2 undergoes a phase transition to a cubic, *Fm*3*m*, β-CsO_2 form.[21] The α-CsO_2 phase shown in Figure 1c was used in this case.[38] In each layer, one cesium atom is coordinated to two oxygen atoms to satisfy the electroneutrality. The crystallographic data and the DFT optimized values for these cesium oxides are summarized in Table 1.

TABLE 1: Unit Cell Parameters for Three Crystal System

	symmetry group	unit cell parameters[43] (Å)	DFT optimized values (Å)
Cs_2O	D_{3d}^5 ($R\bar{3}m$)	$a = 4.256$	$a = 4.256$
		$b = 18.99$	$b = 18.990$
Cs_2O_2	D_{2h}^{25} (*Immm*)	$a = 4.322$	$a = 4.378$
		$b = 7.517$	$b = 7.585$
		$c = 6.430$	$c = 6.616$
CsO_2	D_{4h}^{17} (*I*4/*mmm*)	$a = 4.43$	$a = 4.418$
		$c = 7.20$	$c = 7.447$

TABLE 2: Calculated Bond Lengths in the Three Crystal Systems

crystal system		measured distance (Å)	DFT optimized distance (Å)
Cs_2O	Cs−Cs	4.19[a]	4.256
	Cs−O	2.86[a]	2.844
Cs_2O_2	Cs−Cs	3.79[a]	3.896
	Cs−O	2.95[a]	2.964
	O−O	1.50[a]	1.537
CsO_2	Cs−Cs	4.43[a]	4.418
	Cs−O	3.26[a]	3.046
	O−O	1.30 [b]	1.356

[a] From ref 38. [b] From ref 50.

TABLE 3: Charges and Bond Overlap Populations of Bulk CsO_x Crystals

	O	Cs	Cs−O	Cs−Cs	O−O
Cs_2O	−1.64	0.82	0.16	0.00	0.00
Cs_2O_2	−0.93	0.93	0.02	0.00	0.11
CsO_2	−0.49	0.98	0.00	0.00	0.21

As shown in Table 1, the bulk unit cell volume of Cs_2O_2 and CsO_2 expanded by 3−5% after geometry optimization compared to the experimentally measured unit cell volumes. This is not surprising because the GGA method is known to slightly overestimate bond lengths.[41,42] This small expansion is within the range of error associated with DFT. The method provides an appropriate description of various CsO_x crystal structures. The unit cell volume of Cs_2O did not change significantly. Table 2 compares the distances between cesium and oxygen atoms in different CsO_x crystals. The calculated distances are in good agreement with those measured experimentally, with the largest deviation being less than 5%.

Table 3 reports the Mulliken charges on Cs and O atoms along with the overlap population between these atoms for the Cs_2O, Cs_2O_2, and CsO_2 bulk oxides. The charges on the oxygen

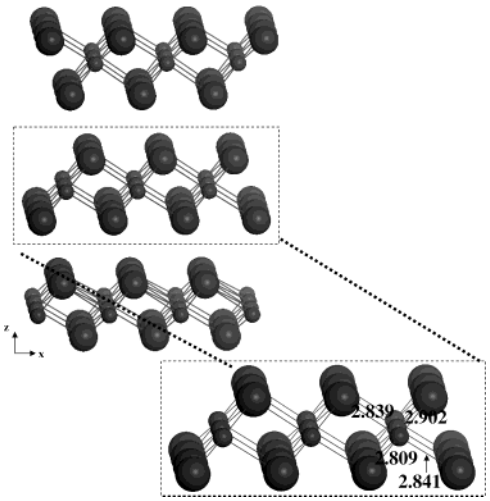

Figure 2. Superstructure and {001} surface of Cs_2O crystal. Distances are in angstroms.

TABLE 4: Surface Energy of CsO_x Surfaces

	cesium oxide compound				
	Cs_2O		Cs_2O_2		CsO_2
surface plane	{001}	{010}	{001}	{100}	{001}
energy ($J \cdot m^{-2}$)	0.00	0.21	0.23	0.78	0.12

atoms indicate that Cs_2O, which has the most negative charge on the oxygen atoms in the crystal structure, is the strongest base, followed by Cs_2O_2, and then CsO_2. The magnitude of the charge on the O atoms in Cs_2O_2 and CsO_2 also reflects the nature of these oxides, with O_2^{2-} and O_2^- present in peroxide and superoxide, respectively. Increasing the oxygen content in the cesium system decreases the overlap population between Cs and O atoms. The O−O overlap in bulk CsO_2 is the largest and the Cs − O overlap was negligible. The calculated O−O bond lengths, 1.56 Å for Cs_2O_2 and 1.36 Å for CsO_2, are typical of those associated with peroxides and superoxides.[43] Because the oxygen atoms in the Cs_2O bulk unit cell are completely surrounded by Cs atoms, there is a negligible O−O bond overlap population. The change of Mulliken charge on O atoms in Cs_2O_2 and CsO_2 can be attributed to the formation of a covalent bond between the two adjacent oxygen atoms in these crystals. The O−O covalent interaction becomes even stronger in the CsO_2 crystal because the O−O overlap population increased from 0.11 in Cs_2O_2 to 0.21. In general, this trend agrees with the results reported by Krawietz et al., which indicated that the stoichiometric alkali metal oxide M_2O exhibits only basic properties whereas the peroxide and superoxide show both basic and oxidative reactivity.[21]

3.2. CsO_x Surfaces. Several low index surfaces were cleaved from the optimized bulk Cs_2O unit cells. The {001} and {010} surfaces of Cs_2O, the {001} and {100} surfaces of Cs_2O_2, and the {100} surface of CsO_2 were found to be stable. Table 4 summarizes the surface energy of these systems.

Four Cs_2O unit cells were placed in a 2×2 fashion along both [100] and [010] directions to create a Cs_2O superstructure as shown in Figure 2. A Cs−O−Cs triple layer was then selected as the exposed plane. As a result, the geometrically optimized {001} surface was terminated with cesium atoms, as seen in Figure 2. The bond distance between surface O and Cs atoms was 2.80 ± 0.05 Å (an average of 2.80 with 0.05 Å of deviation), which is the same bond distance as in the bulk unit cell. The negligible surface energy indicates that the surface is particularly stable.

The {010} surface of the Cs_2O, illustrated in Figure 3a, was also explored. This surface was created by cutting through all three Cs−O−Cs triple layers. Bonds between O and Cs atoms in the bulk unit cell were broken, which resulted in unsaturated surface bonds. Figure 3b shows the surface after relaxation. The surface energy of the optimized configuration is 0.21 $J \cdot m^{-2}$, which is significantly higher than the energy of {001} surface. The optimized surface structure showed that a massive degree of reconstruction is necessary to lower the energy in this system. In particular, discrete Cs_2O units rearranged to form $(Cs_2O)_2$ dimers and the interactions between Cs and O increased accordingly. The bond distance between Cs and O in $(Cs_2O)_2$ dimers decreased from 2.85 ± 0.05 to 2.70 ± 0.03 Å.

To show the influence of underlying layers on the single Cs−O−Cs triple layer structure presented in Figure 3a,b, two additional Cs−O−Cs triple layers were added underneath. The oxygen and cesium atoms in these two layers were fixed at the bulk values whereas the surface atoms were free to relax. Parts c and d of Figure 3 compare the surface before and after geometric relaxation. Instead of forming the $(Cs_2O)_2$ dimer system observed for the single Cs−O−Cs layer, the surface oxygen atoms moved in the $[00\bar{1}]$direction to expose cesium atoms. Cesium atoms also moved as seen in Figure 3d. The addition of underlying cesium oxide layers significantly stabilized the surface.

Two cesium peroxide surfaces were also examined. A Cs_2O_2 slab was constructed from the optimized bulk Cs_2O_2 unit cell. For the {001} surface, the slab was based on three bulk Cs_2O_2 unit cells stacked along the [001] direction. A vacuum spacing of ca. 12 Å was then produced by removing three Cs−O−Cs layers from the slab. The bottom two triple layers in the slab were held fixed and the top triple layer was free to relax. A similar procedure was used to construct the {100} surface. Figures 4 and 5 illustrate the {001} and the {100} surface of Cs_2O_2, respectively. Minor relaxation in the {001} surface included shortening of the Cs−O bond from 2.94 Å in the bulk to 2.89 and 2.91 Å on the surface. The distance between the top O−Cs−O layer and the middle one increased 0.02 Å (from 2.47 to 2.49 Å after relaxation) in the {001} surface. The surface energy of the relaxed {001} surface was calculated to be 0.23 $J \cdot m^{-2}$, whereas that of the relaxed {100} surface was 0.78 $J \cdot m^{-2}$. The Cs_2O_2 {100} surface is therefore less stable than the {001} surface.

The {001}, {100}, and {110} surfaces of CsO_2 were also explored. The {001} surface, shown in Figure 6, was the only surface found to be stable, with a surface energy of 0.12 $J \cdot m^{-2}$. The {001} surface was constructed with three optimized CsO_2 unit cells aligned in the {001} direction, thus forming three triple-layer structures with two oxygen atoms per cesium atom in each layer. Relaxations in the surface layers were negligible; i.e., the bond distance between Cs and O atoms on the surface (3.25 ± 0.05 Å) equaled that in the bulk (3.25 ± 0.05 Å).

3.3. Adsorption of CO_2 on the CsO_x Surfaces. The surface with CO_2 adsorbed was optimized with various sites and adsorption modes to establish the most favorable mode of adsorption and the binding energy (adsorption strength). In general, basic metal oxides adsorb CO_2 strongly by forming surface carbonates. Infrared (IR) spectroscopy indicates that CO_2 is adsorbed on metal oxide surfaces in various configurations, including unidentate, bidentate, and bridged (Scheme 1).[44−47] Carbon dioxide may form unidentate or bidentate carbonates on CsX and CsO_x loaded zeolites, depending on the basic strength of the surface.[44,46] It was suggested that more basic surfaces result in unidentate carbonates whereas less basic

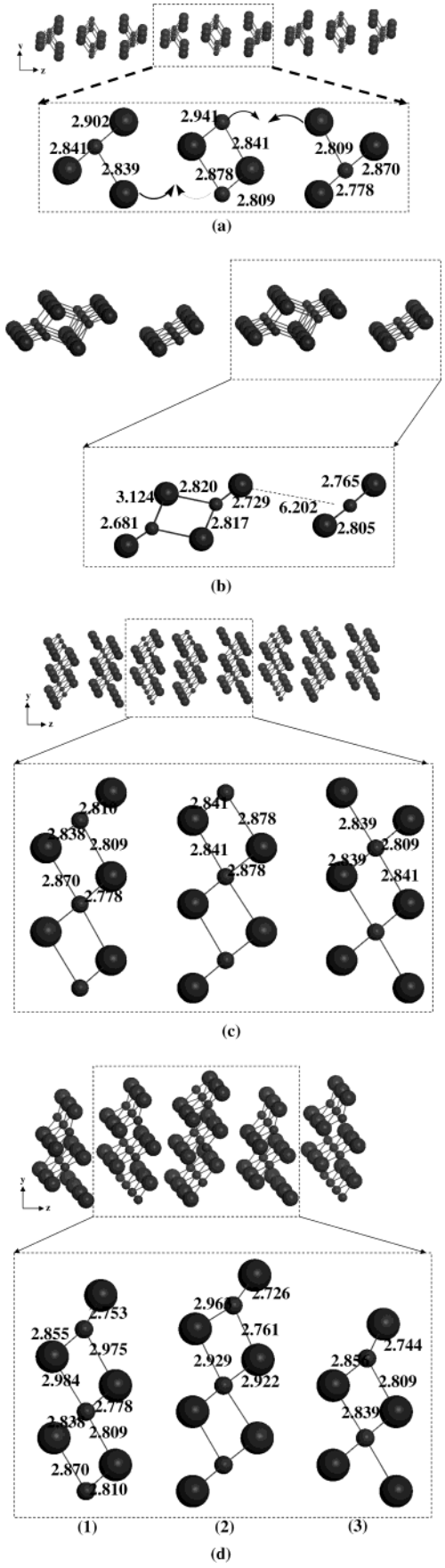

Figure 3. (a) The unrelaxed {010} surface of Cs_2O. The relaxation path is shown by the arrows. (b) The geometrically optimized {010} surface of Cs_2O. (c) Unrelaxed Cs_2O {010} surface with additional layers. (d) Relaxed Cs_2O {010} surface with additional layers. All distances are in angstroms.

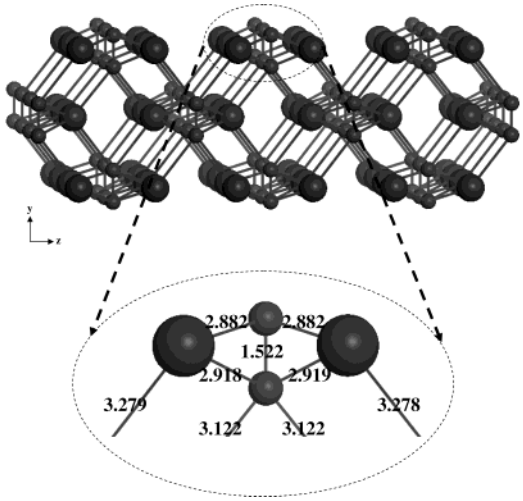

Figure 4. {001} surface of a Cs_2O_2 crystal. Distances are in angstroms.

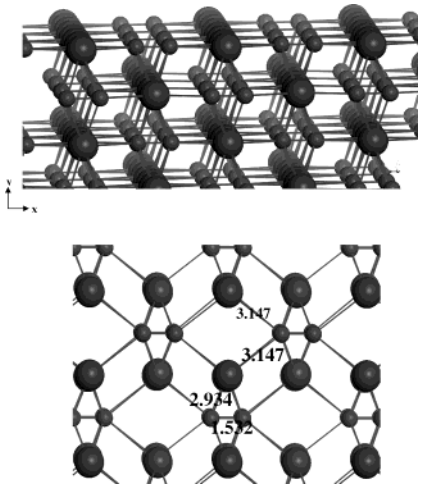

Figure 5. {100} surface of a Cs_2O_2 crystal. Distances are in angstroms.

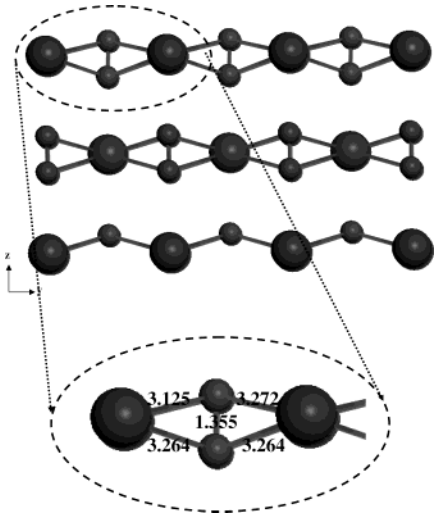

Figure 6. Stable {001} surface of a CsO_2 crystal. Distances are in angstroms.

surfaces result in bidentate carbonates.[44] Thus, multiple configurations were studied in this work. The calculated binding energies for CO_2 on different surfaces studied herein are summarized in Table 5.

The Cs_2O {001} surface, terminated with Cs atoms (Figure 2), was found to be nearly inert to CO_2 adsorption. The very

SCHEME 1: Possible Configurations of Adsorbed CO_2 on the CsOx Surface

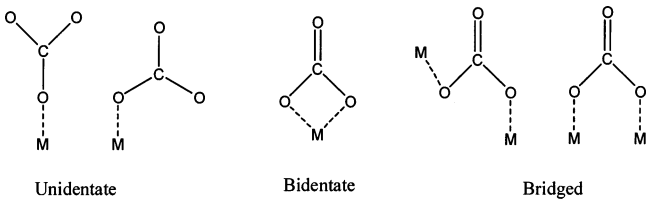

TABLE 5: Adsorption Energy (kJ mol^{-1}) of CO_2 on CsO_x Surfaces

	Cs_2O	
{001}	Cs-terminated surface	−4.1
	unidentate oxidized surface	−95
{010}	bridged	−284
	Cs_2O_2	
{001}	unidentate along [001]	−18
	unidentate along [010]	−19
	unidentate along [110]	−95
	bridged	−101
{100}	unidentate	N/A
	bridged	−186

low binding energy of −4.1 kJ mol^{-1} for the adsorbed CO_2 indicates that the interaction with the surface is weak. A weak interaction is expected because the bare surface is very stable. Indeed, carbon dioxide adsorption induced little change in the structure of the surface. Table 6 shows the Mulliken charge analysis on the CsO_x surfaces before and after CO_2 adsorption. The Mulliken charges on the oxygen and cesium atoms of the Cs_2O {001} surface did not change upon CO_2 adsorption. In the Cs−O−Cs triple layer structure, the oxygen atoms are surrounded completely by Cs atoms. Thus, there is very little interaction between the oxygen atoms buried below the Cs atoms and the C atom of the CO_2 molecule.

The fact that the commercially available "Cs_2O" is actually a mixture of Cs_2O_2 and CsO_2[21] indicates that Cs_2O can be easily oxidized. We therefore explored adsorption of CO_2 over an oxidized Cs_2O surface. An O adatom was introduced on top of the hollow site of the cesium-terminated {001} surface, as illustrated in Figure 7. This is a simple model to help show the interaction of Cs−O sites with CO_2. The influence of including spin polarization in the calculation changed the total energy by only 2 kJ mol^{-1}. Therefore subsequent calculations involving CO_2 adsorption on this surface were performed without spin polarization option. The binding energy of the oxygen adatoms on the Cs_2O {001} surface was calculated according to O_2 (g) → 2O(atoms) to be −141 kJ mol^{-1}, indicating that oxidation of the surface is thermodynamically favorable. The bond distance between the surface O and Cs atoms was found to be 2.50 ± 0.02 Å, which is significantly shorter than the bond length in the bulk (2.85 ± 0.02 Å). Interestingly, the bond distances between the surface Cs atoms and the bulk oxygen atoms were slightly elongated. However, the bulk structure of the Cs_2O crystal underneath the {001} surface was not significantly affected by the introduction of oxygen adatoms. The Mulliken charges of the surface oxygen and cesium atoms on the oxidized Cs_2O {001} surface are summarized in Table 6. The adsorbed oxygen adatom on the surface is bound strongly to the surface atoms. The Mulliken charge on the oxygen adatom (−0.94) is comparable to the surface oxygen atom in the Cs_2O_2 {001} surface (−0.92). The nature of this Cs−O surface bond is fairly ionic, as demonstrated by the Mulliken charge on the oxygen atom. The strong interaction between the surface oxygen and the Cs_2O surface resulted in a local complex similar to that exposed on a Cs_2O_2 surface.

The oxidized surface adsorbs CO_2 in a unidentate configuration with a binding energy of −94.6 kJ mol^{-1} (Figure 8). Compared to the surface before CO_2 adsorption, the bond distance between surface Cs and O elongated from 2.50 ± 0.02 Å to 2.70 and 2.95 Å. The bond distance between C in the CO_2 molecule and a surface oxygen adatom was 1.50 Å. The distance between the surface Cs atoms and the O atoms from CO_2 molecule was 3.05 ± 0.05 Å. In this case, CO_2 is adsorbed onto the oxidized surface, forming a carbonate species. The "oxidized Cs {001} surface" model shows that surface Cs−O pairs are needed to interact strongly with CO_2.

In contrast to the inert, cesium-terminated {001} surface, the stoichiometric {010} surface is much more active for adsorption of CO_2, as shown in Figure 9a. The binding energy is −284 kJ mol^{-1}, which is very close to the measured value of −270 kJ mol^{-1} at 373 K on a commercial "Cs_2O" sample that was pretreated at 623 K for 5 h under vacuum.[20] The high reactivity of the {010} surface is consistent with its high surface energy, 0.21 J·m^2. Adsorption of CO_2 induced a massive degree of surface reconstruction. The bond between the carbon atom and the surface oxygen atom was 1.33 Å, which is close to the bond distance between the carbon atom and the two oxygen atoms in the CO_2 molecule (1.29 Å). Thus the adsorbed species appeared to be similar to a bridged carbonate species. The Mulliken charge on a surface oxygen atom changed from −1.67 to −1.49 whereas the charge on a Cs atom decreased from 0.83 to 0.73, as summarized in Table 6. The rearrangement of the surface forms new $(Cs_2O)_2$ dimers, which redistribute the charges of surface Cs and O atoms.

To test the influence of slab thickness on the adsorption of CO_2 molecules, two Cs−O−Cs layers were added below the Cs_2O {010} surface as illustrated in Figure 9b. The CO_2 adsorption energy on the supported Cs_2O {010} surface was calculated to be −268 kJ mol^{-1}, which agrees well with the adsorption energy on the single layer slab, and even closer to the experimentally measured −270 kJ mol^{-1}. In summary, these results show that the surface of Cs_2O has a high affinity for CO_2 if both cesium and oxygen atoms are available for bonding.

The adsorption of CO_2 on the Cs_2O_2 surfaces discussed earlier was examined. Three different unidentate configurations and two bridged configurations were explored. Figure 10 illustrated a typical unidentate configuration of CO_2 molecule on the Cs_2O_2 {001} surface. The CO_2 molecule was placed in a unidentate configuration along the [100], [010], and [110] directions on the Cs_2O_2 {001} surface. Figure 11 shows CO_2 adsorbed in a bridged configuration on the Cs_2O_2 {001} surface.

The adsorption of CO_2 in a unidentate configuration originally aligned in the [100] and [010] directions on the {001} surface was weakly bound, resulting in a binding energy of −20 kJ mol^{-1}. However, the adsorption energy increased to −95 kJ mol^{-1} with the alignment of CO_2 along the [110] direction. The bridged configuration gave a binding energy of −101 kJ mol^{-1}. As expected, the bridged configuration had a stronger interaction with the surface than the unidentate configuration.

The bond distance between the carbon atom of CO_2 and the surface O atom originally adsorbed along the [100] and [010] directions was 2.30 ± 0.05 Å. The shorter C−O surface bond distance for CO_2 bound unidentate along the [110] direction (1.481 Å) and for bridged-bound CO_2 (1.421 Å) is consistent with the higher binding energy of those systems. The distance between the oxygen atoms of the CO_2 molecule and the surface cesium atoms was calculated to be 3.0 Å for the [110] aligned unidentate structure, and 2.9 Å for the bridged structure. Each

TABLE 6: Charges and Overlap Population of Various CsO_x Surfaces[a]

		CO_2 adsorption	O	Cs	Cs−Cs	O−O	Cs−O
Cs_2O	Cs terminated {001} surface	before	−1.64	0.82	0.00	0.00	0.06
		after	−1.63	0.81	0.00	0.00	0.06
	oxidized {001} surface	before	−0.94	0.91	0.00	0.10	0.00
		after	−0.93	0.91	0.00	0.09	0.00
	{010} surface	before	−1.67	0.83	0.00	0.00	0.09
		after	−1.49	0.73	0.00	0.00	0.00
Cs_2O_2	{001} surface	before	−0.92	0.94	0.00	0.09	0.03
		after	−0.81	0.67	0.00	0.14	0.00
	{100} surface	before	−0.93	0.94	0.00	0.12	0.00
		after	−0.85	0.92	0.00	0.10	0.02

[a] The surfaces were geometrically optimized prior adsorption of CO_2 and denoted as "before" in the Table whereas the "after" surfaces were those after the adsorption of CO_2 and subsequent relaxation. The charge analysis was performed on surface atoms only. The CO_2 molecule was not used in the charge analysis. The charge analysis was not performed on any of the CsO_2 surfaces because none of them adsorb CO_2 favorably.

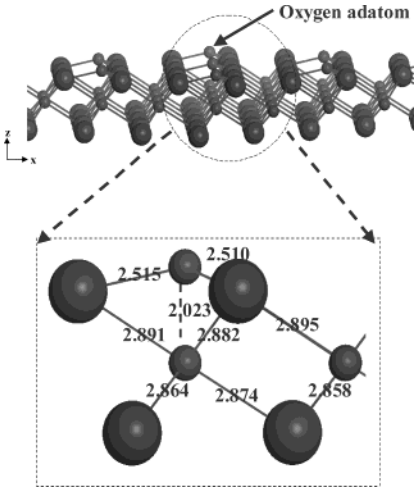

Figure 7. Oxidized {001} surface of a Cs_2O crystal. Distances are in angstroms.

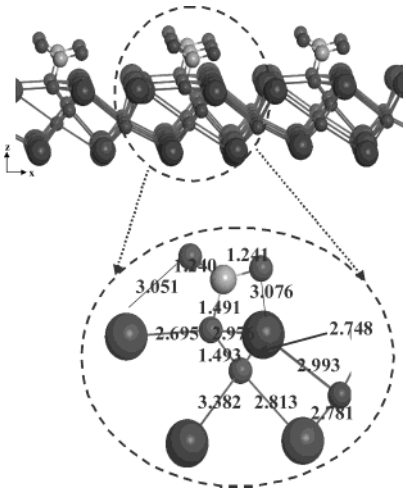

Figure 8. Oxidized {001} surface of Cs_2O with adsorbed CO_2 molecules. Distances are in angstroms.

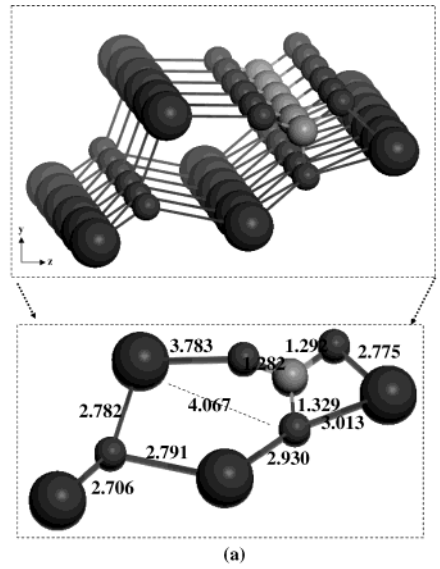

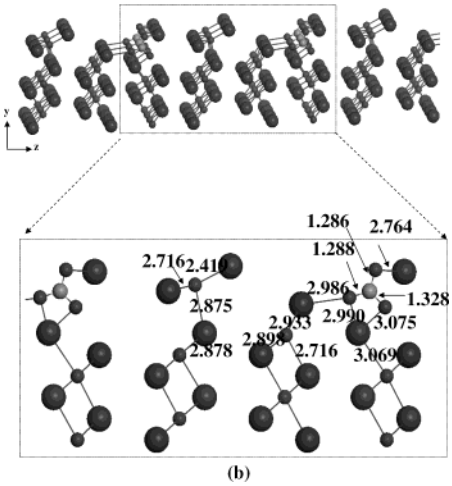

Figure 9. (a) {010} surface of Cs_2O with adsorbed CO_2. (b) Adsorption of CO_2 on Cs_2O {010} surface with additional layers. All distances are in angstroms.

cesium atom on the surface is coordinated to three oxygen atoms. The unidentate configuration along the [110] direction and the bridged configuration are qualitatively and quantitatively quite similar to one another.

The adsorption of CO_2 on the {001} surface of Cs_2O_2 resulted in a significant rearrangement of the surface atoms. The O−O pair in the surface of Cs_2O_2 significantly rearranges due to adsorption of CO_2. The dioxygen pair in the {001} surface moved from a 90° orientation (vertical with respect to the {001} surface) to 41.9° in the [110] aligned unidentate model, and from 90° to 50.2° in the bridged model. The orientation of Cs atoms in the {001} surface moved from horizontal positions to 15.4° in the [110] aligned unidentate model, and 60.5° in bridged model.

The optimized structure for bridged-bound CO_2 adsorbed on the {100} surface of Cs_2O_2 is shown in Figure 12. The binding energy of CO_2 in this configuration was calculated to be −186 kJ mol^{-1}, which is considerably stronger than the binding energy for CO_2 on the {001} surface. The calculations with CO_2 starting

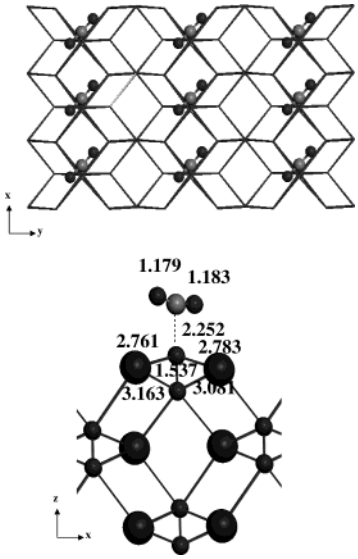

Figure 10. Top view of the optimized unidentate CO_2 molecule on the {001} surface of Cs_2O_2. The CO_2 molecule was originally aligned in the [100] direction. Distances are in angstroms.

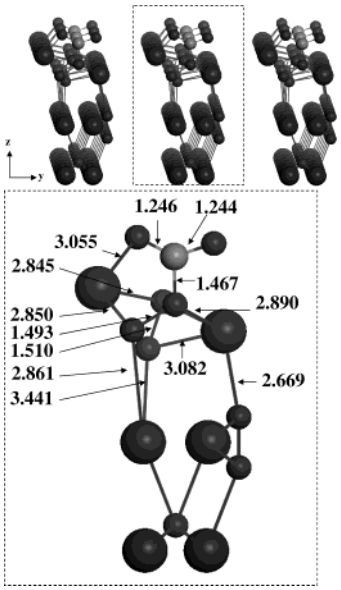

Figure 11. Side view of the bridged CO_2 molecule on the {001} surface of Cs_2O_2 crystal (low coverage). Distances are in angstroms.

from a unidentate configuration on the {100} surface did not lead to converged results.

Attempts were also made to optimize CO_2 adsorption on the {001} surface of a CsO_2 crystal, but the results indicated that CO_2 did not bind the surface.

On the basis of the results presented here, cesium superoxide (CsO_2) can be excluded as an active species for the adsorption of CO_2. Both Cs_2O and Cs_2O_2, however, exhibit a strong affinity for CO_2 adsorption. Surface reconstruction was observed upon the adsorption of CO_2 on the Cs_2O {010} surface and both peroxide surfaces examined here. In a study on high-temperature vaporization behavior of alkali metal oxides, Lamoreaux and Hildenbrand found that, in an oxygen deficient environment ($P_{O_2} \approx 10^{-15}$ bar) and at temperatures below 620 K, Cs_2O_2 is the stable surface structure, whereas above 630 K, Cs_2O is more stable.[48] In an oxygen rich environment ($P_{O_2} = 0.2$ bar), CsO_2 is the stable species. This finding is consistent with our oxygen adsorption calculations, which showed that Cs_2O could be easily oxidized.

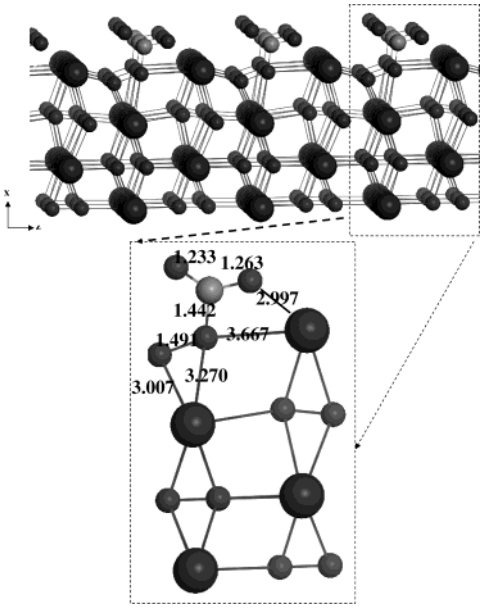

Figure 12. Side view of the bridged CO_2 molecule on the {100} surface of Cs_2O_2 crystal. Distances are in angstroms.

Lasperas et al.,[18] Rodriguez et al.,[49] and Kim et al.[47] have suggested that Cs_2O species are formed inside the micropores of zeolites after the decomposition of cesium precursors. However, the enthalpy of CO_2 adsorption on the occluded cesium species was only about -85 kJ mol^{-1}.[20] From the results presented here, adsorption of CO_2 on Cs_2O should have a much stronger adsorption energy than -85 kJ mol^{-1}. Cesium peroxide is a possible candidate for the occluded species in the zeolites. An EXAFS study on cesium-modified zeolites reported that the average Cs$-$O distance is 2.94 ± 0.03 Å,[44] which is close to the Cs$-$O distance found here for Cs_2O_2 (3.00 ± 0.05 Å). The computed Cs$-$O distances in Cs_2O (2.80 ± 0.05 Å) and CsO_2 (3.25 ± 0.05 Å) are outside of the range of Cs$-$O distances from EXAFS results. However, our current results do not exclude the possibility that other compounds such as oxycarbonates are present in the supported species in zeolites.

4. Conclusions

The low index surfaces of Cs_2O required exposed Cs and O atoms to interact with CO_2. Thus, adatoms of oxygen on an inert cesium-terminated surface activate the surface toward CO_2 adsorption. If both Cs and O are exposed on stoichiometric Cs_2O, CO_2 is adsorbed with an energy of -284 kJ mol^{-1}, which is a substantially stronger interaction than that found on Cs_2O_2 (up to -186 kJ mol^{-1}) or CsO_2 (no adsorption). The very high adsorption energy on Cs_2O is comparable to that reported for the experimentally measured ΔH_{ads} on a commercial cesium oxide sample after thermal activation.[20] Substantial reconstruction of the clean and CO_2 covered surfaces compared to the bulk crystal was observed in several cases.

Acknowledgment. We thank the Department of Energy (Basic Energy Sciences, Grant DEFG02-95ER14549) for the financial support. Calculations were carried out on the sp2 computer clusters, which are owned by the University of Virginia.

References and Notes

(1) Gregory, P. E.; Chye, P.; Sunami, H.; Spicer, W. E. *J. Appl. Phys.* **1975**, *46*, 3525.
(2) Ebbinghaus, G.; Simon, A. *J. Appl. Phys.* **1979**, *50*, 8252.

(3) Sommer, A. H. *J. Appl. Phys.* **1980**, *51*, 1254.
(4) Phillips, C. C.; Hughes, A. E.; Sibbett, W. *J. Phys. D Appl. Phys.* **1984**, *17*, 611.
(5) Woratschek, B.; Sesselmann, W.; Kuppers, J.; Ertl, G.; Haberland, H. *J. Chem. Phys.* **1987**, *86*, 2411.
(6) Pedio, M.; Benfatto, M.; Aminpirooz, S.; Haase, J. *Phys. Rev. B* **1994**, *50*, 6596.
(7) Weitkamp, J.; Hunger, M.; Rymsa, U. *Microporous Mesoporous Mater.* **2001**, *48*, 255.
(8) Hattori, H. *Chem. Rev.* **1995**, *95*, 537.
(9) Lackner, K. S. *Science* **2003**, *300*, 1677.
(10) Xu, X. C.; Song, C. S.; Andresen, J. M.; Miller, B. G.; Scaroni, A. W. *Energy Fuels* **2002**, *16*, 1463.
(11) Siriwardane, R. V.; Shen, M. S.; Fisher, E. P.; Poston, J. A. *Energy Fuels* **2001**, *15*, 279.
(12) Davis, R. J. *J. Catal.* **2003**, *216*, 396.
(13) Kloetstra, K. R.; van den Broek, J.; van Bekkum, H. *Catal. Lett.* **1997**, *47*, 235.
(14) Hathaway, P. E.; Davis, M. E. *J. Catal.* **1989**, *116*, 263.
(15) Hathaway, P. E.; Davis, M. E. *J. Catal.* **1989**, *119*, 497.
(16) Tu, M.; Davis, R. J. *J. Catal.* **2001**, *199*, 85.
(17) Yagi, F.; Hattori, H. *Microporous Mater.* **1997**, *9*, 247.
(18) Lasperas, M.; Cambon, H.; Brunel, D.; Rodriguez, I.; Geneste, P. *Microporous Mater.* **1993**, *1*, 343.
(19) Hathaway, P. E.; Davis, M. E. *J. Catal.* **1989**, *116*, 279.
(20) Bordawekar, S. V.; Davis, R. J. *J. Catal.* **2000**, *189*, 79.
(21) Krawietz, T. R.; Murray, D. K.; Haw, J. F. *J. Phys. Chem. A* **1998**, *102*, 8779.
(22) Sauer, J.; Ugliengo, P.; Garrone, E.; Saunders, V. R. *Chem. Rev.* **1994**, *94*, 2095.
(23) Pacchioni, G. *Heterogeneous Chem. Rev.* **1995**, *2*, 213.
(24) Whitten, J. L.; Yang, H. *Surf. Sci. Rep.* **1996**, *24*, 59.
(25) Hammer, B.; Norskov, J. K. *Adv. Catal.* **2000**, *45*, 71.
(26) Stampfl, C.; Ganduglia-Pirovano, M. V.; Reuter, K.; Scheffler, M. *Surf. Sci.* **2002**, *500*, 368.
(27) van Santen, R. A.; Neurock, M. *Encyclopedia of Catalysis*; Wiley: New York, 2001.
(28) van Santen, R. A.; Neurock, M. *Catal. Rev. Sci. Eng.* **1995**, *37*, 557.
(29) Ge, Q. F.; Kose, R.; King, D. A. *Adv. Catal.* **2000**, *45*, 207.
(30) Accelrys, I. *Materials Studio CASTEP*, 2.1 ed.; Accelrys Inc.: San Diego, 2001.
(31) Milman, V.; Winkler, B.; White, J. A.; Pickard, C. J.; Payne, M. C.; Akhmatskaya, E. V.; Nobes, R. H. *Int. J. Quantum Chem.* **2000**, *77*, 895.
(32) Payne, M. C.; Teter, M. P.; Allan, D. C.; Arias, T. A.; Joannopoulos, J. D. *Rev. Mod. Phys.* **1992**, *64*, 1045.
(33) Vanderbilt, D. *Phys. Rev. B* **1990**, *41*, 7892.
(34) Perdew, J. P.; Chevary, J. A.; Vosko, S. H.; Jackson, A. K.; Pederson, R. M.; Singh, D. J.; Fiolhais, C. *Phys. Rev. B* **1992**, *46*, 6671.
(35) *CRC Handbook of Chemistry and Physics*, 73rd ed.; Lide, D. R., Ed.; CRC Press: Boca Raton, FL, 1993.
(36) Monkhorst, H. J.; Pack, J. D. *Phys. Rev. B* **1976**, *13*, 5188.
(37) Mulliken, R. S. *J. Chem. Phys.* **1955**, *23*, 1833.
(38) Wyckoff, R. W. G. *Crystal Structures*, 2nd ed.; Interscience Publisher: New York, 1963; Vol. 1.
(39) Tsai, K. R.; Harris, P. M.; Lassettre, E. N. *J. Phys. Chem.* **1956**, *60*, 338.
(40) Foppl, V. H. *Anorg. Allg. Chem.* **1957**, *291*, 12.
(41) Rozanska, X.; Demuth, T.; Hutschka, F.; Hafner, J.; van Santen, R. A. *J. Phys. Chem. B* **2001**, *106*, 3248.
(42) Jeanvoine, Y.; Angyan, J. G.; Kresse, G.; Hafner, J. *J. Phys. Chem. B* **1998**, *102*, 5573.
(43) Wells, A. F. *Structural Inorganic Chemistry*, 3rd ed.; Oxford University Press: Oxford, U.K., 1962.
(44) Doskocil, E. J.; Davis, R. J. *J. Catal.* **1999**, *188*, 353.
(45) Lavalley, J. C. *Catal. Today* **1996**, *27*, 377.
(46) Turek, A. M.; Wachs, I. E. *J. Phys. Chem.* **1992**, *96*, 5000.
(47) Kim, J. C.; Li, H. X.; Chen, C. Y.; Davis, M. E. *Microporous Mater.* **1994**, *2*, 413.
(48) Lamoreaux, R. H.; Hildenbrand, D. L. *J. Phys. Chem. Ref. Data* **1984**, *13*, 151.
(49) Rodriguez, I.; Cambon, H.; Brunel, D.; Lasperas, M.; Geneste, P. *Heterogeneous Catal. Fine Chemicals III* **1993**, 623.
(50) Vanerberg, N. G. *Prog. Inorg. Chem.* **1962**, *4*, 125.